



UPDATED CONSTANT STRESS DROP SCALING RELATIONSHIP FOR STRIKE-SLIP EARTHQUAKES CONSIDERING FAULT SLIP RATE

John G. Anderson⁽¹⁾, Glenn P. Biasi⁽²⁾, Stephen Angster⁽³⁾, Steven G. Wesnousky⁽⁴⁾

⁽¹⁾ Professor, University of Nevada, jga@unr.edu

⁽²⁾ Research Associate Professor, University of Nevada Reno; now at US Geological Survey, Pasadena, gbiasi@usgs.gov

⁽³⁾ Research Assistant, University of Nevada, Reno; now at US Geological Survey, Seattle, sangster@nevada.unr.edu

⁽⁴⁾ Professor, University of Nevada, stevew@seismo.unr.edu

Abstract

Anderson et al. [1] proposed a scaling model to estimate magnitude of earthquakes from the fault length that suggested a systematic dependence on the slip rate. This model was superseded by Anderson et al. [2] based on an expanded data set, in which slip-rate dependence is significant for strike-slip faults, but not resolved for normal or reverse faulting. This study extends those results for strike-slip earthquakes. The goal of the model presented here is to correlate average slip and rupture width with rupture length, reduce the misfit, and assure that parameters are internally consistent with the definition of the seismic moment.

We proceed by extending the database of [2] to include estimates of mean surface slip and down-dip rupture width. We then modify model M3 of [2]. M3 is a closed-form equation with constant stress drop to estimate the mean magnitude for strike-slip earthquakes. The equation can accommodate independent rupture lengths and widths, but in M3 a mean backbone scaling relationship was obtained using an estimate of the rupture width as a function of the rupture length. Ultimately, we conclude that the width is too uncertain to use as a regression parameter in developing the updated model. Thus, a likelihood method is adopted: the likelihood of the model fitting both magnitude and slip for each earthquake is calculated for a two-dimensional grid of points defined by all reasonable values of width and stress drop. The events are then grouped by ranges of rupture length, and the likelihood of each combination of width and stress drop is determined for the group. As expected, the contours of these likelihoods show a strong tradeoff between width and stress drop: larger stress drop on thinner faults is difficult to distinguish from smaller stress drop on wider faults. Based on seismological observations that the stress drop is relatively independent of magnitude, we find the maximum likelihood width for each group of rupture length that is consistent with a constant stress drop. The trade-off is resolved by requiring that the widths should be reasonably consistent with the compiled estimates. This approach prevents any possibility that, with increased length, the stress drop can increase to unphysical values. The preferred backbone model, which we designate as M4, reduces the standard deviation of the misfit to observed magnitudes compared to model M3. Surprisingly, the most likely values of width are proportional to $\log(\text{length})$.

Next, we confirm that the slip rate reduces the uncertainty in estimates of the magnitude in model M4. This is a specific case of what could be a more general search for additional physically observable parameters that might reduce the uncertainty in scaling relations.

[1] Anderson, J., Wesnousky, S. & Stirling, M. Earthquake size as a function of fault slip rate. *Bulletin of the Seismological Society of America* 86, 683–690 (1996).

[2] Anderson, J. G., Biasi, G. P. & Wesnousky, S. G. Fault scaling relationships depend on the average fault slip rate. *Bulletin of the Seismological Society of America* 107, 2561–2577 (2017).

Keywords: earthquake; faulting; scaling; seismic hazard; seismicity



1. Introduction

An essential component for seismic hazard analysis is the use of fault scaling relations to estimate magnitude (M_W) based on geological and geophysical observations of the dimension of an active fault. A complete seismicity model includes the magnitudes and rates of all earthquakes that are relevant to the hazard at the site that is under study. The seismic hazard analysis combines the magnitude and fault geometry with the distance to the site to estimate the ground motion at the site. These two groups of information are rigorously combined to develop the site hazard curve. Geological observations are the best way to estimate the magnitude of possible earthquakes on the fault. They can provide the fault location, length of the observed surface trace and a sense of motion, the slip rate on the fault, and also sometimes an estimate of the local surface slip in one or more recent earthquakes. Geophysical data may give some insight on the depth of brittle faulting. The scaling relationship uses these parameters to estimate the magnitude of a possible earthquake [e.g. 5].

Several recent studies [e.g. 6, 7] have reviewed the history of scaling relations, so there is no need to repeat that in detail. It has long been recognized that rupture area [e.g. 8, 9] or rupture length [e.g. 10, 11] are correlated with the magnitude. The correlations are understood based on our understanding of earthquake physics [12, 2].

Anderson, Wesnousky and Stirling [1], superseded by Anderson, Biasi, and Wesnousky [2] (subsequently referred to as ABW17) suggested an extension of this model by considering the effect of fault slip rate on fault scaling. ABW17 concluded that for strike-slip faults, the geological slip rate of the fault can significantly reduce the uncertainty in the estimates of M_W . They also proposed one model, M3, which appeared to predict the data well with a constant stress drop, based on the stress drop definition of Chinnery [3, 4]. This was an encouraging result, since teleseismic observations usually show that there is not a large variation in the stress drop of earthquakes over very large magnitude ranges [e.g. 13, 14, 15]. Possible magnitude dependence may be due to imperfections in the sensitive adjustments for attenuation [e.g. 16, 17]. However, ABW17 did not collect information on the average coseismic slip or fault width for the earthquakes that were used.

This paper evaluates whether the M3 constant stress-drop model to estimate M_W from fault length and slip rate can be improved to provide estimates of average slip by incorporating an improved model for the fault width and stress drop. The addition of a model for the width that is consistent with average slip (D_E) and M_W increases the usefulness of this model for generating synthetic seismograms and for estimates of fault displacement hazard. This paper only considers earthquakes that have predominantly a strike-slip focal mechanism. As seen by ABW17, the available data for earthquakes with predominantly reverse or normal mechanisms is not well distributed for a study of this nature, and furthermore may not be consistent with the slip-rate dependence found for strike-slip events.

2 Background

2.1 Seismic moment and moment magnitude

Seismic moment, (M_0), is defined as

$$M_0 = \mu L_E W_E D_E \quad (1)$$

where L_E is the rupture length in the earthquake, W_E is the rupture width of the earthquake, D_E is the average slip on the fault during the earthquake, and μ is the shear modulus. Let S_F be the geological slip rate of the fault. The magnitude is considered to be essentially a transformation of variables from the seismic moment, using the equation that is implicit in Kanamori ([18]):

$$M_W = \frac{2}{3} \log \left[\frac{M_0}{M_0(0)} \right] \quad (2)$$



where $M_0(0)$ is the seismic moment of an earthquake with moment magnitude of zero, $10^{16.1}$ dyne-cm or $10^{9.1}$ Newton-meters [19, 20, 21]. This paper uses units consistent with $\log M_0(0) = 16.1$, since those are used by the Global CMT Project.

2.2 ABW17 M3

ABW17 discussed three scaling relations to estimate M_w from L_E and S_F , the geological slip rate of the fault. The primary interest of this paper is their model labeled M3, which is motivated by equations from Chinnery [3, 4]. The M3 equations are:

$$M_0 = \frac{2\pi}{C(\gamma)} \Delta\tau_C L_E W_E^2 \quad (3)$$

Where

$$C(\gamma) = 2 \cos \gamma + 3 \tan \gamma - \frac{\cos \gamma \sin \gamma (3 + 4 \sin \gamma)}{(1 + \sin \gamma)^2} \quad (4)$$

and

$$\tan \gamma = \frac{2W_E}{L_E} \quad (5)$$

The stress drop parameter, $\Delta\tau_C$, identified by Chinnery [3, 4], gives the stress drop at the top center of a rectangular fault that ruptures the surface and has uniform slip over its entire surface. We note the similarity in form of Equation 3 and equations in Figure 1 of Kanamori and Anderson [12], that give the moment for three other fault and slip geometries with analytical expressions for stress drop. The magnitude scaling in M3 is written explicitly by substituting Equation 3 into Equation 2, and adding the term $c_2 \log(S_F/S_0)$ to adjust the magnitude for slip rate. Table 1 summarizes the parameters suggested by ABW17 for model M3. The function $C(\gamma)$ modulates a transition in the slope of the scaling between $\sim 2 \log L_E$ when the fault size increases with no change in aspect ratio to $(2/3) \log L_E$ for a long fault where ruptures may increase in length with no change in width. For a fault approaching infinite length, $\Delta\tau_C = \Delta\tau_{KA}/2$ where $\Delta\tau_{KA}$ is the stress drop given by Kanamori and Anderson [12] for a long strike slip fault with the same slip at the surface.

A benchmark for this study is the standard deviations of the magnitude residuals in model M3 (Table 1).

3 Data

3.1 Criteria for Data Selection

Earthquakes were considered for this study if reliable, independent measurements are available for the rupture length (L_E), average slip (D_E), seismic moment (M_0), and long-term, average slip rate on the fault (S_F). We initially also sought estimates of the width of faulting (W_E), but in the end this was treated as an unknown parameter to be optimized for use in Equation 3. The observational estimates of W_E are highly scattered, and when estimated by the distance from the surface to the maximum depth of aftershocks, they may be much wider than the depth range of patches of maximum slip. Much of the information on M_w , L_E , and S_F is the same as used by ABW17, although updating of estimates occurred in many cases. To be specific, M_0 is based on the Global CMT project, local catalogs, and published evaluations. The rupture length L_E is the length of the ruptured zone, from end to end. This and D_E are mainly from geological studies. L_E can be a small-circle length as for the 2002 Denali earthquake in Alaska. This approach does not count the lengths of secondary ruptures that splay off from the main fault (e.g. Canterbury, Bulnay). The near-surface materials need to be regarded as highly variable and highly nonlinear, so surface slip gives an imperfect representation of the deeper slip on the fault below. With this in mind, geological slip estimated from the upper bound of plots of slip along the fault trace are considered, in this study, to be most representative of slip at depth, but still are likely to be smaller than the slip at depth, especially for the shorter ruptures. A complete summary of this work is given by Anderson et al. [22].



4 Properties of the data

The data used in this study are summarized in Anderson et al. [22]. Figure 1 shows locations of the considered earthquakes. The selected events occur in western United States, Guatemala, countries in the Middle East, China, Mongolia, Russia, Japan, the Philippines, and New Zealand. Figure 2 shows that the observed rupture lengths are spread relatively uniformly over a range of distances from 15 to 500 km.

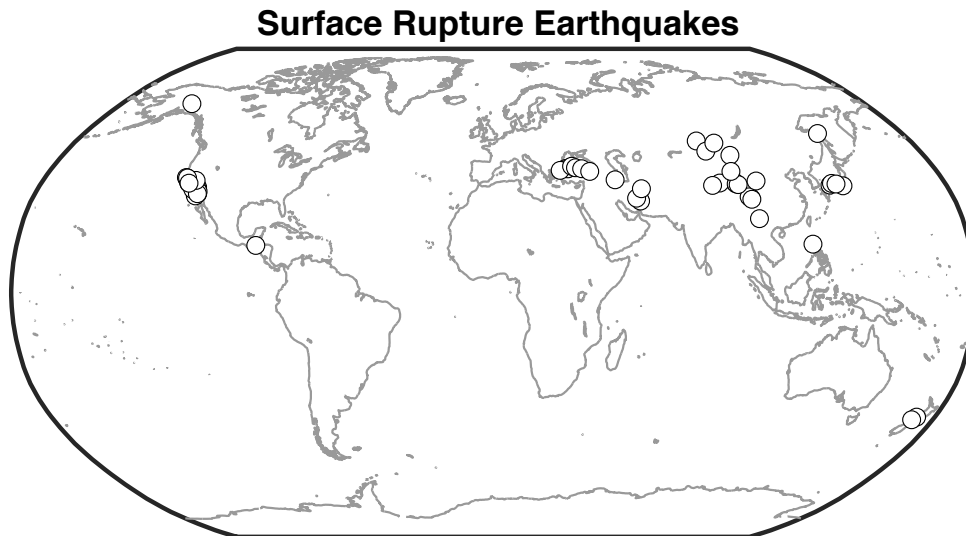


Figure 1: Locations of strike-slip earthquake included in this study.

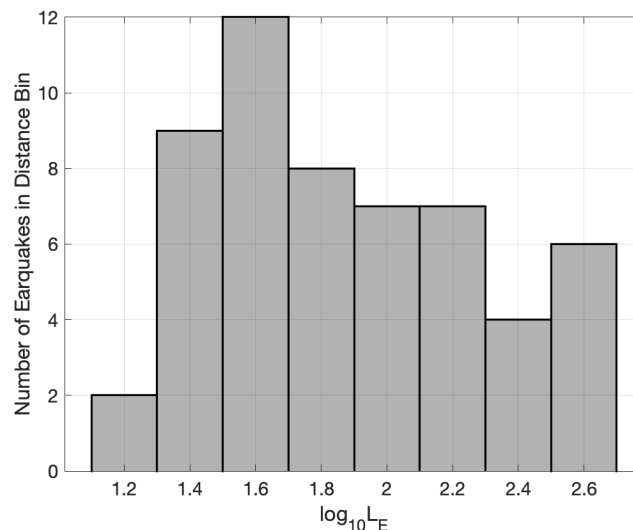


Figure 2: Distribution of rupture lengths for the considered earthquakes.

5 Maximum Likelihood Approach and Results

The problem of finding optimum values of $\Delta\tau_C$ and W_E is best approached using maximum likelihood methods. Two likelihood functions were found for each earthquake, one for the likelihood of a model predicting M_w and the other for the likelihood of the model predicting L_E .

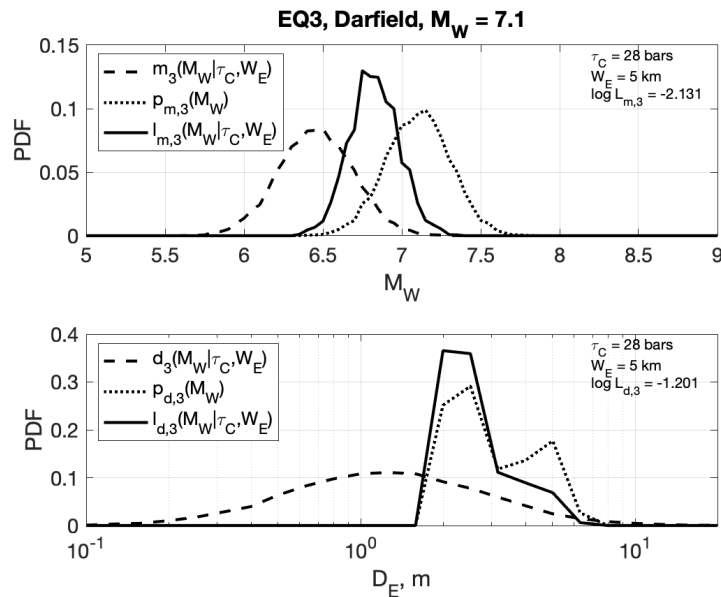


Figure 3: Darfield earthquake: Likelihood calculation for $\Delta\tau_C = 28$ bars and $W_E = 5$ km.

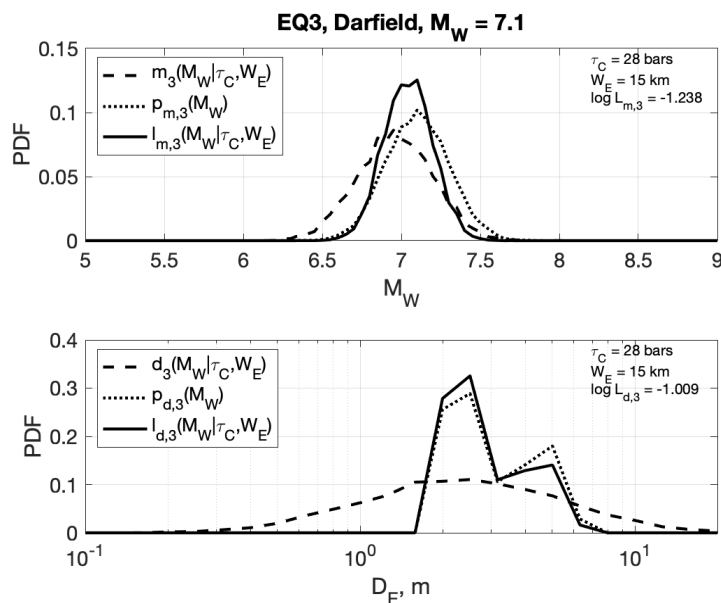


Figure 4: Darfield earthquake: Likelihood calculation for $\Delta\tau_C = 28$ bars and $W_E = 15$ km.

Figure 3 illustrates the calculation that was applied to each earthquake. It shows the steps taken to estimate the likelihood that a particular model, defined by selected values of $\Delta\tau_C$ and W_E , is consistent with observations of the 2010 Darfield, New Zealand earthquake. The observed magnitude and slip are $M_W = 7.1$ and $D_E = 2.55$ m [22]. A probability distribution for the observed magnitude, $p_{m,i}(M_W)$ is shown with the dotted lines in the upper frame. The index i identifies the earthquake. A corresponding distribution $p_{d,i}(D_E)$ is shown in the lower frame for observed slip. For the slip, the uncertainty range [22] is 1.9-5.8 m. To account for this uncertainty range, both $p_{m,i}(M_W)$ and $p_{d,i}(D_E)$ assume that the best estimate is the median of the distribution. The 50% probability of larger magnitude or slip is distributed uniformly between the median and the maximum value. Similarly, the 50% probability of smaller magnitude or slip is distributed uniformly between the median and the minimum value. The dashed lines below and above the median slip are sloped



because the horizontal axis is logarithmic, while $p_{d,i}(DE)$ is drawn on a linear scale. The uncertainties in the observed M_W are further expanded with an additional uncertainty modeled by a normal distribution function with uncertainty of 0.2 magnitude units. Because the distributions of $p_{m,i}(M_W)$ and $p_{d,i}(DE)$ do not all easily lend themselves to an analytical form, they are estimated by 10,000 Monte-Carlo trials following the rules just described.

The distribution of the model for the magnitude, $m_i(M_W | \Delta\tau_C, W_E)$, is based on Equation 3 for each trial value of $\Delta\tau_C$ and W_E . The uncertainty in this estimate is assumed to be the same as in M3, i.e. $\sigma_{3L}=0.236$ (Table 1). The corresponding density for the slip, $d_i(DE | \Delta\tau_C, W_E)$, is found using Equations 1 and 2. These model distributions are shown as dashed lines in Figure 3.

The likelihood density functions, are then found as

$$l_{m,i}(M_W | \tau_C, W_E) = p_{m,i}(M_W) m_i(M_W | \tau_C, W_E) \quad (6)$$

and

$$l_{d,i}(DE | \tau_C, W_E) = p_{d,i}(DE) d_i(DE | \tau_C, W_E) \quad (7)$$

These density functions have been normalized to unit area in Figures 3, in order to enhance visibility, but in reality their areas are much smaller. Their areas under the curves given by Equations 6 and 7 are the likelihoods that the selected values of $\Delta\tau_C$ and W_E fit the magnitude and slip of earthquake i . The equations are:

$$L_{m,i}(\tau_C, W_E) = \int l_{m,i}(M_W | \tau_C, W_E) dM_W \quad (8)$$

and

$$L_{d,i}(\tau_C, W_E) = \int l_{d,i}(DE | \tau_C, W_E) dDE \quad (9)$$

The logarithms of these likelihoods are given in the respective frames of Figure 3. Giving magnitude and slip estimates equal weight, the total likelihood of earthquake i being modeled by Equation 3 with selected values of $\Delta\tau_C$ and W_E is given by

$$\log [L_i(\tau_C, W_E)] = \log [L_{m,i}(\tau_C, W_E)] + \log [L_{d,i}(\tau_C, W_E)] \quad (10)$$

Figures 3 and 4 illustrate the effect of changing the trial fault width for constant $\Delta\tau_C = 28$ bars. In Figure 3, the model and observed magnitudes are not aligned, so the likelihood of this model for estimating the magnitude is less than 10^{-2} . In contrast, when W_E is increased to 15 km, the predicted and observed magnitudes are substantially aligned, and the likelihood is increased. The range of DE predicted by the model is quite wide, so the likelihood of fitting DE is somewhat less selective, but it still shows a preference for the 15 km width.

Evaluating the likelihoods of events of similar rupture length is useful. Figure 2 shows the distribution of the numbers of earthquakes in each of eight groups of rupture lengths. For group g , where g varies from 1 to 8, representing in sequence the eight groups in Figure 2, the likelihood of each tested model of $\Delta\tau_C$ and W_E is

$$\log L_g(\tau_C, W_E) = \sum_{i \in g} \log L_i(\tau_C, W_E) \quad (11)$$

The likelihoods in Equation 11 can be contoured, and in principle, the combination of $\Delta\tau_C$ and W_E with the highest value is the best model for this group.

The contours for two sample length ranges are shown in Figures 5 and 6. Two features are immediately obvious. The first is that stress drop and rupture width are strongly correlated, such that a larger width and low stress drop can have nearly the same likelihood as a small width and larger stress drop. The tradeoff is not linear as seen by the curvature of the ridges in Figures 5 and 6. The second point is that the tradeoff is quite different for the two selected ranges of rupture length.



Given the seismological observation that stress drop is relatively independent of magnitude, vertical profiles from Figures 5, 6, and the other six length ranges were investigated. The profiles at $\Delta\tau_C = 28$ bars are also shown in Figures 5 and 6. To find the width with the maximum likelihood along each profile, likelihoods between the calculated points near the peak were estimated using a cubic spline (Matlab function 'interp1' with the 'cubic' interpolation method). Uncertainties were estimated by, rather arbitrarily, finding the width of the peak at 75% of the peak value.

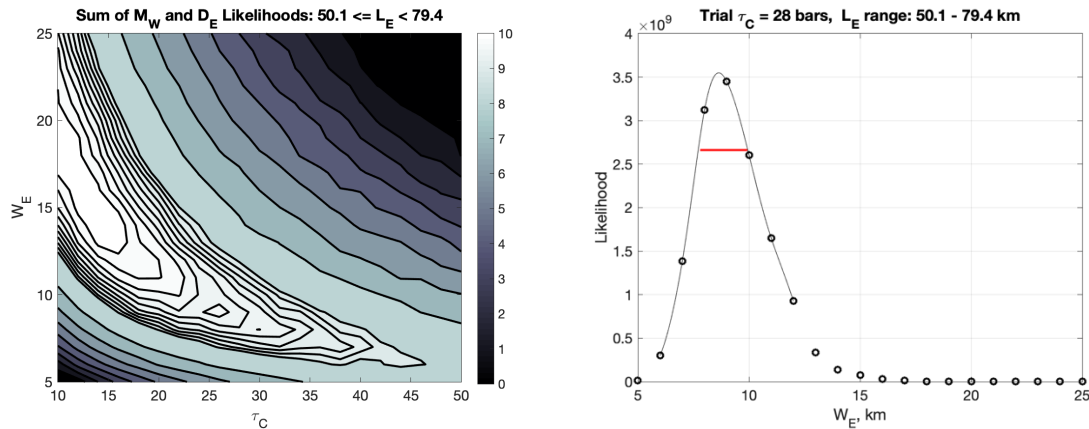


Figure 5: Left: Contours of model likelihoods, on a logarithmic scale, for events with rupture lengths from 50-79 km. Values are normalized for a peak likelihood of 10^{10} . Right: Vertical profile of the contours, on a linear scale, at $\Delta\tau_C = 28$ bars.

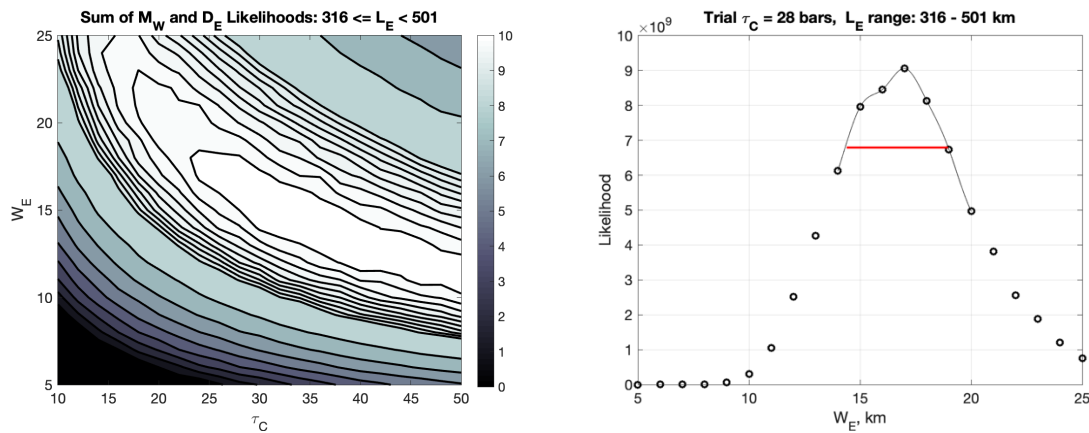


Figure 6. Equivalent to Figure 5, for events with rupture lengths from 315-500 km.

The peaks and uncertainties from the profiles in Figures 5 and 6, and also the other rupture length bands, are shown in Figure 7. In Figure 7, the rupture widths determined by the maximum likelihood method are proportional to the log of the rupture length. The relationship found is

$$W_E = 11.6 + 8.63 \log \left(\frac{L_E}{100} \right) \quad (12)$$

with units of L_E and W_E in kilometers.

The quality of the agreement between the maximum likelihood widths and the model described in Equation 12 is both striking and surprising. For instance, Leonard (2010) developed a set of self-consistent scaling models based on the assumption that $W_E \sim L_E^\beta$. For the points in Figure 7, the best-fitting power law relationship (not shown in the figure) has a misfit, $\sigma_w = 1.01$ km that is substantially larger than $\sigma_w = 0.69$ for the log-linear model that is shown in Figure 7. Models with the same form as Equation 12, but different coefficients, were consistently superior to power law models for all considered alternative values of $\Delta\tau_C$.



With these considerations, this study pursues the use of Equation 12 to estimate of W_E for scaling based on Equation 3.

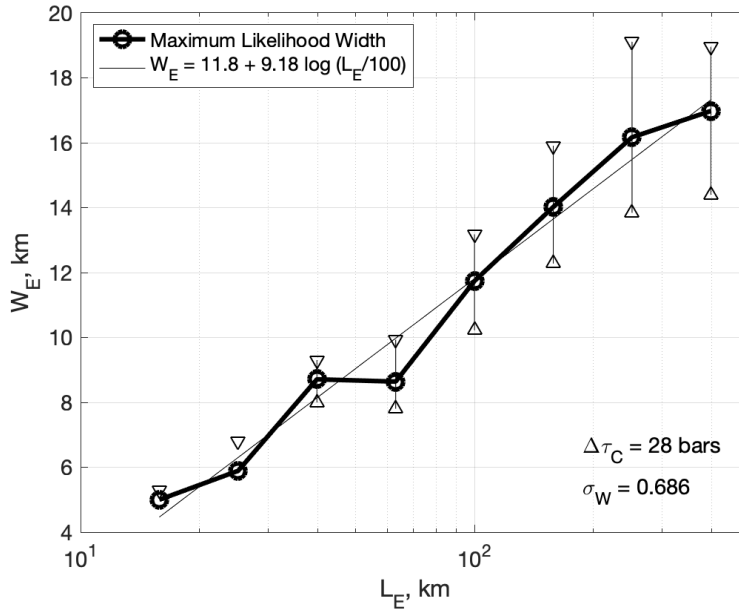


Figure 7: Estimated rupture widths as a function of rupture length for $\Delta\tau_C = 28$ bars.

6 Evaluation

Equation 3, using Equation 12 to estimate the fault width as a function of the length, is our improved scaling model, and we shall identify it as Model M4. Figure 8 compares the prediction of the model with the fault width data. The widths for large rupture lengths are consistent with the observations, and this rough consistency is the motivation for the choice of $\Delta\tau_C = 28$ bars. The agreement is unimpressive for short ruptures. Figure 9 compares the mean slip predictions of the model with the preferred surface slip from Tables 2 and 3. As for rupture width estimates, the observations are generally consistent with observations for large events, but the agreement is poor for short rupture lengths. These discrepancies will be discussed subsequently.

Using Equation 12, Figure 10 shows estimated magnitudes as a function of the rupture length. In this case, the agreement of model and data appears to be satisfactory. Residuals from the trend in Figure 10 are shown in Figure 11 as a function of length, and in Figure 12 as a function of slip rate. A least-squares fit to the residuals in Figure 11 is not significantly different from zero. The least-squares fit to the residuals in Figure 12 finds that

$$\delta M_W = -0.213 \log \left(\frac{S_F}{S_0} \right) \quad (13)$$

where $S_0 = 6.1$ mm/yr. This confirms the previous result of ABW17, that for strike-slip faults a higher slip rate is significantly correlated with a more negative residual. The slope of the linear regression in Figure 12 is slightly greater than the slope found in ABW17 (Table 1). Table 1 also shows the residuals of this new model and the corresponding residuals from M3 of ABW17. The uncertainty in predicting the magnitude from length alone is slightly decreased with use of Model M4, and more significantly decreased when predicting the magnitude using both length and slip rate.



Table 1: Parameters for Models M3 and M4 for strike-slip earthquakes
Common features of both models:

$$M_0 = \frac{2\pi}{C(\gamma)} \Delta\tau_C L_E W_E^2$$

$$M_W = \frac{2}{3} \log \left[\frac{M_0}{M_0(0)} \right] + c_2 \log \left[\frac{S_F}{S_0} \right]$$

Property	Model M3	Model M4
W_E (km)	15 for ($L_E > 57$ km) $L_E/3.8$ for ($L_E \leq 57$ km)	$11.8 + 9.18 \log \left(\frac{L_E}{100} \right)$
$\Delta\tau_C$	24.9 ± 1.1 bars	28 bars
c_2	-0.170 ± 0.029	-0.216 ± 0.042
S_0	4.8 mm/yr	6.1 mm/yr
σ_L	0.236	0.227
σ_S	0.214	0.186

$M_0(0) = 10^{16.1}$ dyne-cm or $10^{9.1}$ Newton-meters, the moment of an earthquake with magnitude $M_W = 0$.

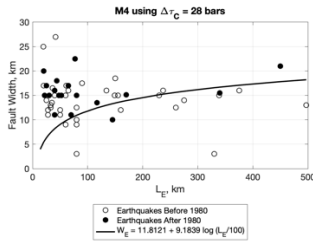


Figure 8: Width from Length model & data.

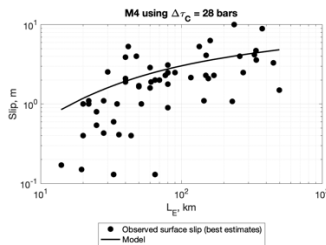


Figure 9: Best estimates of surface slip from rupture length, based on model M4.

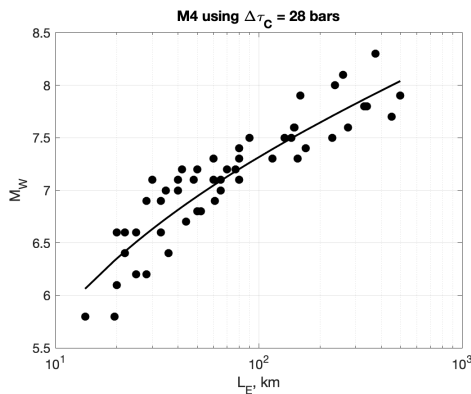


Figure 10: Magnitude from rupture length for $\Delta\tau_c=28$ bars.

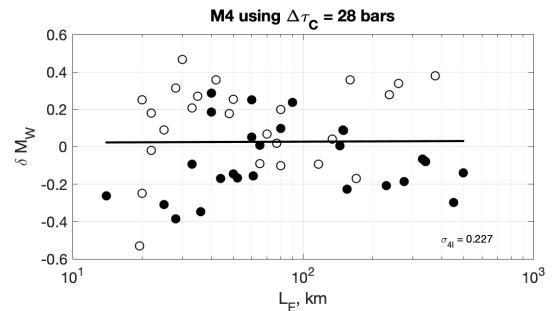


Figure 11: Magnitude residuals vs length

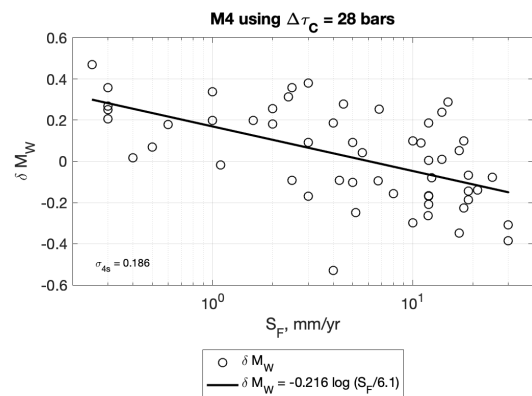


Figure 12: Magnitude residuals vs. slip rate



7 Discussion and Conclusions

The primary advantages of Model M4 compared with Model M3 is that it fits our data set better, and that M4 is also designed to provide a self-consistent model for the rupture length and slip. This is achieved by the major assumption that the stress drop, $\Delta\tau_c$ is constant and subsequently finding an empirical relationship from the data between L_E and W_E . Before applying the adjustment for slip rate, Model M4 is self-consistent, in the sense that given any one of the parameters M_W , L_E , W_E , or D_E , the other three are uniquely estimated. This self-consistent property might appear to break down when the perturbation for the slip rate S_F is added. However, this perturbation can be uniquely mapped into a perturbation to the stress drop, in which case the self-consistency of the other parameters will still hold.

An alternative approach to selecting model parameters could be to select a constant value of W_E , and then find optimum values of $\Delta\tau_c$ to model the data. This approach would find that the stress drop is an increasing function of the rupture length. An argument might even be made for its reasonableness, considering that stresses may be lower for surface-rupturing earthquakes than for events that are deeper. From the perspective of a modeling exercise, such a model would do about as well as the adopted approach. However, because constant stress drop is reasonably well supported by the teleseismic observations (e.g. [13]), this study has not investigated this alternative approach.

The relationship between W_E and L_E in Equation 12 was not expected. An interesting question is whether there is any theoretical justification for a log-linear relationship of this nature. Based on Figure 8, Equation 12 does not seem to fit the observed values of W_E particularly well. However, we suggest that the small rupture widths at small magnitudes are not unreasonable. The best estimates are often assumed from the maximum depths of aftershocks. However, inversions for slip distributions have often found that the majority of slip on the faults takes place in patches over a smaller depth range than the width of the seismogenic zone. For example, for the Yushu earthquake ($M_W 6.8$, $L_E = 50$ km) Yang et al., [23] found aftershocks to ~ 13 km depth, but the largest slip patch found by waveform inversion extends from the surface to ~ 7 km depth, and is thus quite consistent with Equation 12. We note also that width W_E in Equation 1 refers to the width that contributes to elastic energy in the main shock, which for moderate earthquakes is likely to be concentrated at asperities. For that reason, for the present, we decided not to pursue a model that provides a better fit to the scattered fault width and surface slip data.

There are some obvious possible extensions to this model. Clearly the database can be extended. One limiting factor is availability of geologically constrained slip rates, but it seems inevitable that more observations of this type will be developed. It is reasonable to expect that W_E is correlated with the heat flow, where a higher heat flow would be expected to correlate with a smaller fault width. Another potential correlation could be with the thickness of the continental crust, where a thicker crust could correlate with lower heat flow, and thus larger fault widths. These ideas are left for future study.

Acknowledgements

Research supported by the U.S. Geological Survey (USGS), Department of the Interior, under USGS award number G17AP00105. The views and conclusions contained in this document are those of the authors and should not be interpreted as necessarily representing the official policies, either expressed or implied, of the U.S. Government.

References

- [1] Anderson, J., Wesnousky, S. & Stirling, M. Earthquake size as a function of fault slip rate. *Bulletin of the Seismological Society of America* 86, 683–690 (1996).
- [2] Anderson, J. G., Biasi, G. P. & Wesnousky, S. G. Fault scaling relationships depend on the average fault slip rate. *Bulletin of the Seismological Society of America* 107, 2561–2577 (2017).
- [3] Chinnery, M. A. The stress changes that accompany strike-slip faulting. *Bulletin of the Seismological Society of America* 53, 921–932 (1963).
- [4] Chinnery, M. A. The strength of the earth's crust under horizontal shear stress. *Journal of Geophysical Research* 59 (1964).



- [5] Field, E. H. et al. Uniform California earthquake rupture forecast, version 3 (UCERF3)—the time-independent model. *Bulletin of the Seismological Society of America* 104, 1122–1180 (2014).
- [6] Leonard, M. Earthquake fault scaling: self-consistent relating of rupture length, width, average displacement, and moment release. *Bulletin of the Seismological Society of America* 100, 1971–1988 (2010).
- [7] Hanks, T. C. & Bakun, W. H. M–log A models and other curiosities. *Bulletin of the Seismological Society of America* 104, 2604–2610 (2014).
- [8] Wyss, M. & Brune, J. N. Seismic moment, stress, and source dimensions for earthquakes in the California-Nevada region. *Journal of Geophysical Research* 73, 4681–4694 (1968).
- [9] Hanks, T. C. & Bakun, W. H. M–log A observations for recent large earthquakes. *Bulletin of the Seismological Society of America* 98, 490–494 (2008).
- [10] Tocher, D. Earthquake energy and ground breakage. *Bulletin of the Seismological Society of America* 48, 147–153 (1958).
- [11] Wells, D. L. & Coppersmith, K. J. New empirical relationships among magnitude, rupture length, rupture width, rupture area, and surface displacement. *Bulletin of the Seismological Society of America* 84, 974–1002 (1994).
- [12] Kanamori, H. & Anderson, D. L. Theoretical basis of some empirical relations in seismology. *Bulletin of the Seismological Society of America* 65, 1073–1095 (1975).
- [13] Allmann, B. P. & Shearer, P. M. Global variations of stress drop for moderate to large earthquakes. *Journal of Geophysical Research* 114, B01310 (2009).
- [14] Baltay, A. G., Prieto, G. & Beroza, G. C. Radiated seismic energy from coda measurements and no scaling in apparent stress with seismic moment. *Journal of Geophysical Research-Solid Earth* 115, B08314 (2010).
- [15] Baltay, A., Ide, S., Prieto, G. & Beroza, G. C. Variability in earthquake stress drop and apparent stress. *Geophysical Research Letters* 38, L06303 (2011).
- [16] Anderson, J. G. Implication of attenuation for studies of the earthquake source. *Geophysical Monograph* 37, (Maurice Ewing Series 6), 311–318 (1986).
- [17] Abercrombie, R. Earthquake source scaling relationships from -1 to 5 M_L using seismograms recorded at 2.5-km depth. *Journal of Geophysical Research-Solid Earth* 100, 24,015–24,036 (1995).
- [18] Kanamori, H. The energy release in great earthquakes. *Journal of Geophysical Research* 82, 2981–2987 (1977).
- [19] IASPEI. Summary of magnitude working group recommendations on standard procedures for determining earthquake magnitudes from digital data. Tech. Rep., International Association for Seismology and Physics of the Earth's Interior (2005).
- [20] IASPEI. Summary of magnitude working group recommendations on standard procedures for determining earthquake magnitudes from digital data. Tech. Rep., International Association for Seismology and Physics of the Earth's Interior (2013).
- [21] Bormann, P., Wendt, S. & DiGiacomo, D. Chapter 3. Seismic sources and source parameters. In Bormann, P. (ed.) *New Manual of Seismological Observatory Practice 2 (NMSOP2)*, 1–259 (Deutsches GeoForschungsZentrum GFZ, Potsdam, 2013).
- [22] Anderson, J. G., Wesnousky, S. G., Biasi, G. P. & Angster, S. Scaling relationships for seismic moment and average slip of strike-slip earthquakes incorporating fault slip rate and maximum likelihood values of fault width and stress drop. *Bulletin of the Seismological Society of America* in review (2020).
- [23] Yang, W., Peng, Z., Wang, B., Li, Z. & Yuan, S. Velocity contrast along the rupture zone of the 2010 Mw6.9 Yushu, China, earthquake from fault zone head waves. *Earth and Planetary Science Letters* 416, 91–97 (2015).